ISSN 1810-2328, Journal of Engineering Thermophysics, 2019, Vol. 28, No. 1, pp. 26–42. © Pleiades Publishing, Ltd., 2019.

Constructal Design of Conductive Asymmetric Tri-Forked Pathways

T. M. Fagundes[1], G. Lorenzini[2*], E. da S. D. Estrada[3], L. A. Isoldi[3], E. D. dos Santos[3], L. A. O. Rocha[4], and A. J. da Silva Neto[5]

[1]*Department of Mechanical Engineering, Universidade Federal do Rio Grande do Sul, Rua Sarmento Leite, 425, Porto Alegre, RS, 90050-170 Brazil*

[2]*Universita degli Studi di Parma, Dipartimento di Ingegneria e Architettura, Parco Area delle Scienze 181/A, 43124 Parma, Italy*

[3]*School of Engineering, Universidade Federal do Rio Grande, Italia Avenue km 8, Rio Grande, RS, 96201-900 Brazil*

[4]*Mechanical Engineering Graduaate Program, Universidade do Vale do Rio dos Sinos—UNISINOS, Av. Unisinos, 950, CEP 93022-750, Sao Leopoldo, RS, Brazil*

[5]*Polytechnic Institute, Universidade do Estado do Rio de Janeiro UERJ, Nova Friburgo, RJ, Brazil*

Received September 3, 2018

Abstract—This work relies on the constructal design method associated with exhaustive search and genetic algorithms to perform geometric optimization of an asymmetric tri-forked pathway of highly conductive materials (inserts) that remove a constant heat flux from a body and deliver it to three isothermal heat sinks. It is shown numerically that the global thermal resistance, represented by the maximum excess of temperature, can be minimized by means of geometric evaluation subject to two constraints, the total rectangular area where the forked pathway is circumscribed and the tri-forked pathway area, and seven degrees of freedom. A parametric study is performed to show the influence of the degrees of freedom over the global thermal resistance. The optimal geometry was obtained for a 40% area fraction, leading to a maximum excess temperature seven-times minimized with a thermal performance 627% better than a once optimized architecture, showing the importance of the design for thermal performance. For higher values of aspect ratio, height/length, the optimal configuration is highly asymmetrical, while for lower ratios the bifurcated branches has low influence over the thermal performance of the system. The optimal tri-forked pathway presented a 307% lower thermal global resistance compared to a V-shaped pathway on the same conditions.

DOI: 10.1134/S181023281901003X

1. INTRODUCTION

The constructal law dictates the universal phenomenon of generation and evolution of design (pattern, shape, structure). This phenomenon is observed in both animate and inanimate systems. Along with the first and second law, the constructal law elevates thermodynamics to a science of systems configuration [1–3]. It has been applied successfully to find shapes that facilitate the flow in animate and inanimate systems [4–9].

The constructal law shows that, besides the conventional "arrow" of time given by the second law of thermodynamics, there is another one for flow organization. This flow organization arrow has been presented since the birth of thermodynamics, but it was not recognized until recently, with the advent of the constructal law [10]. In macroscopic terms, this is the physics of the phenomenon of design, the natural tendency of flow systems to evolve into configurations that provide greater access over time [11].

Bejan et al. [5] showed that the configurations of things found in nature are arranged in such a way that maximize the flow through it, and that the constructal law can predict such configurations. Furthermore, they showed that this phenomenon can be transposed to the engineering field, in applications

*E-mail: giulio.lorenzini@unipr.it

such as renewable energy, refrigeration, heat exchangers, convection, among others [12–18], where the optimal configuration is the one that can evolve into smaller and more complex structures, thus allowing more flow through it.

This link between engineering and the constructal law has been widely discussed. according to Reis and Bejan [6], the constructal law dictates the rules for the best geometry in all scales, showing that these rules are derived from a physical principle and not simply assumed a priori.

Fins have been vastly studied with constructal design. Assemblies of plate and cylindrical T-shaped fins were first studied by Bejan and Almogbel [19]. With the increasing advancements in computers and processors, more complex geometries were studied, now using numerical models instead of analytical solutions. The performance of Y-shaped fin assemblies was analyzed by Lorenzini and Rocha [20] and better results were observed for the optimized Y-shaped geometry, comparing to the previous T-shaped form. Moreover, a T-Y fin assembly with a cavity between the two branches was studied by the same authors [21], showing that a smaller cavity volume and larger fins volume improve the system performance. Twice Y-shaped fins were analyzed by Xie et al. [22] corresponding to a geometry with six degrees of freedom. This twice Y-shaped structure had a thermal performance 36.7% better than the single Y-shaped fin.

One of the applications for the constructal theory in engineering was the study of conduction pathways. Since the early 2000s, several geometries of conduction pathways were studied. For instance, X-shaped conduction pathways within a square-shaped box were studied. Results showed that, for larger values of area fraction, the X-shaped configuration performed 51% better than the I-shaped configuration [23]. Afterwards, even more complex geometries were studied in [24], such as 'phi'- and 'psi'-shaped pathways, obtaining even better configurations, reducing the global thermal resistance in 46% compared to the previously mentioned X-shaped configuration.

Concerning heat conduction through highly conductive materials utilizing the constructal design, an application for heat generating systems was studied, with several geometries being analyzed. Y-shaped pathways with different conductivities of the root and branch sections were studied, distributing the hot spots on the body uniformly and obtaining an improvement of 30% over the Y-shaped pathways with uniform body conductivity [25]. In other scope, a topological analysis of conduction pathways was performed, defining an optimal topology utilizing a nonlimited volume of solid (VoS) function and using it to define a finite geometry limited by conduction pathways of the system [26], while some studies considered the contact resistance in I- and T-shaped bodies [27, 28]. Recent studies also analyzed the influence of conductive pathways in bodies with nonuniform heat generation [29].

The shape variation on symmetric and asymmetric high-conductive trees affects the overall thermal conductance of a heat generating domain, showing that asymmetric boundary conditions induce the geometries to become asymmetric to achieve the best configurations [30]. This effect is observed in a study of an asymmetric V-shaped pathway [31], which determined numerically the best configurations considering constant heat flow being dissipated by two heat sinks on the extremities of the branches. Highly asymmetric geometries were obtained, allowing for a better heat flow through the pathway. These configurations were determined for various volume fraction values relying on the constructal design and Genetic Algorithm.

Based on that V-shaped pathway, this work proposes the optimization of an asymmetric system with one more heat sink in the middle of the system, a tri-forked pathway, which at the best authors knowledge, has not been presented in the literature yet. Besides the new heat sink, this tri-forked pathway was designed with the same boundary conditions as the previous work, for the sake of the optimal geometries comparison.

2. MATHEMATICAL MODEL

Consider the tri-forked pathway sketched in Fig. 1. It receives a constant heat flux delivered to the body at the bottom, i.e., $y = 0$ and $-D_0/2 \leq x \leq D_0/2$, which is conducted through the body. Heat is removed through the end of the three branches that are in touch with heat sinks. Two sinks are located at the top boundary surface of the domain, i.e., $y = H$, and one is at the right boundary surface, i.e., $x = L/2$. The pathway configuration for heat transfer analysis is two-dimensional, with a third dimension (W) sufficiently long in comparison to H and L, allowing those to define the area where the tri-forked pathway is inserted. The heat transfer rate through the root section (q_1) and the temperature

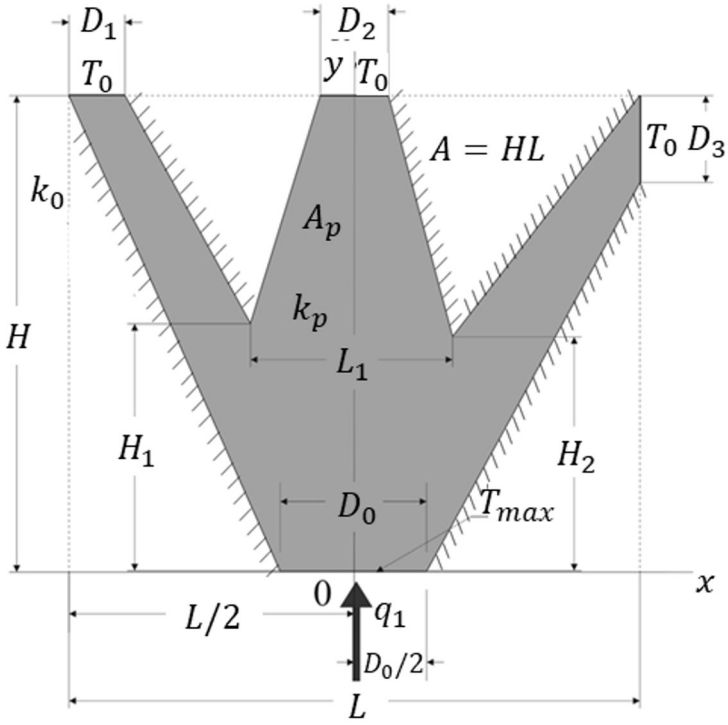

Fig. 1. Tri-forked pathway geometry domain.

of the sinks (T_0) are known. The maximum temperature (T_{max}) occurs at the root section ($y = 0$) and its value varies with the geometry.

The objective of the analysis is to determine the optimal geometry parameters (D_0, D_1, D_2, D_3, H_1, H_2, L_1, H, and L) for a given value of area ratio (φ) that is characterized by the dimensionless minimum global thermal resistance $(T_{max} - T_0)/q_1$. According to constructal design, this optimization is subjected to two constraints, namely, the total area (i.e., the area where the tri-forked high conductive pathway is inscribed) constraint,

$$A = HL, \tag{1}$$

and the pathway area constraint,

$$A_p = \frac{HD_0}{2} + \frac{LH_1}{4} + \frac{HD_1}{2} - \frac{H_1D_1}{2} + \frac{HD_2}{2} - \frac{H_1D_2}{4} + \frac{LH_2}{4} - \frac{H_2D_2}{4} + \frac{LD_3}{4} - \frac{D_3D_0}{4}, \tag{2}$$

where the subscript p means pathways, which can be expressed as a fin volume fraction

$$\varphi = A_p/A. \tag{3}$$

The analysis that gives the global thermal resistance as a function of geometry consists in numerically solving the heat conduction equation along the tri-forked pathway where the pathways are considered isotropic with constant thermal conductivity k_p:

$$\frac{\partial^2\theta}{\partial\tilde{x}^2} + \frac{\partial^2\theta}{\partial\tilde{y}^2} = 0, \tag{4}$$

where the dimensionless variables are

$$\theta = \frac{T - T_0}{q_1/k_p W} \tag{5}$$

and

$$\tilde{x}, \tilde{y}, \tilde{D}_0, \tilde{D}_1, \tilde{D}_2, \tilde{D}_3, \tilde{H}, \tilde{L}, \tilde{H}_1, \tilde{H}_2 = \frac{x, y, D_0, D_1, D_2, D_3, H, L, H_1, H_2}{A^{1/2}}. \tag{6}$$

The boundary conditions for the domain shown in Fig. 1 are given by

$$\frac{\partial \theta}{\partial \tilde{y}} = -\frac{1}{\tilde{D}_0} \text{ at } -\frac{\tilde{D}_0}{2} \le \tilde{x} \le \frac{\tilde{D}_0}{2} \text{ and } \tilde{y} = 0, \tag{7}$$

and

$$\theta = 0 \text{ at the sinks of length } \tilde{D}_1,\ \tilde{D}_2 \text{ and } \tilde{D}_3, \tag{8}$$

and

$$\frac{\partial \theta}{\partial \tilde{n}} = 0 \text{ at the other surfaces (adiabatic)}, \tag{9}$$

where $\tilde{n}$ is the normal unit outward vector to the boundary surface.

The dimensionless forms of Eqs. (1) and (3) are thus defined as

$$1 = \tilde{H}\tilde{L}, \tag{10}$$

$$\varphi = \frac{\tilde{H}\tilde{D}_0}{2} + \frac{\tilde{L}\tilde{H}_1}{4} + \frac{\tilde{H}\tilde{D}_1}{2} - \frac{\tilde{H}_1\tilde{D}_1}{2} + \frac{\tilde{H}\tilde{D}_2}{2} - \frac{\tilde{H}_1\tilde{D}_2}{4} + \frac{\tilde{L}\tilde{H}_2}{4} - \frac{\tilde{H}_2\tilde{D}_2}{4} + \frac{\tilde{L}\tilde{D}_3}{4} - \frac{\tilde{D}_3\tilde{D}_0}{4}. \tag{11}$$

The maximum excess of temperature, θ_{max}, is also the dimensionless global thermal resistance of the construct,

$$\theta_{max} = \frac{T_{max} - T_0}{q_1/k_p W}. \tag{12}$$

2.1. Degrees of Freedom

To find the optimal geometry, the definition of the degrees of freedom for the optimization becomes necessary. These degrees of freedom are dimensionless, thus being more general for future analysis. For the purposes of this work, seven degrees of freedom were chosen for further optimization: $\tilde{D}_0$, D_1/D_0, D_2/D_0, D_3/D_0, H_2/D_0, L_1/D_0, and H/L. With each of these degrees of freedom optimized, added with φ, the optimal geometry of the system can be fully defined.

Table 1. Numerical mesh grid convergence ($\varphi = 0.4$, $\tilde{D}_0 = 0.2$, $D_1/D_0 = D_2/D_0 = D_3/D_0 = 0.5$, $H/L = 0.5$, $L_1/D_0 = 0.4$, $H_2/D_0 = 0.5$)

Number of elements	θ^j_{max}	$\lvert(\theta^j_{max} - \theta^{j+1}_{max})/\theta^j_{max}\rvert$
67	1.8877	1.85×10^{-2}
348	1.9232	6.25×10^{-3}
1392	1.9353	2.42×10^{-3}
5568	1.9400	8.24×10^{-4}
22272	1.9416	—

3. NUMERICAL MODEL

The function defined by Eq. (12) can be determined numerically, by solving Eq. (4) for the temperature field in every assumed configuration of degrees of freedom: $\tilde{D}_0$, D_1/D_0, D_2/D_0, D_3/D_0, H_2/D_0, L_1/D_0, and H/L (for a given φ), and calculating θ_{max} to see whether its value can be minimized by varying the configuration. In this sense, Eq. (4) was solved using a finite element code, based on triangular elements, developed in the MATLAB package, precisely the PDE (partial-differential-equations) toolbox [32, 33]. The mesh grid was nonuniform in both $\tilde{x}$ and $\tilde{y}$ spatial coordinates, and varied from one geometry to the next. The appropriate mesh size was determined by successive refinements, increasing the number of elements four times from one mesh size to the next mesh size, until the criterion $\lvert(\theta^j_{max} - \theta^{j+1}_{max})/\theta^j_{max}\rvert < 1 \times 10^{-3}$ was satisfied. Here θ^j_{max} represents the maximum temperature calculated using the current mesh size, and θ^{j+1}_{max} corresponds to the maximum temperature using the next, for which the number of elements was increased four times. Table 1 gives an example on how the grid independence was obtained. The following results were performed by using a range from 2,000 to 10,000 triangular elements.

Concerning the accuracy of the numerical code, the numerical results obtained using the code in MATLAB PDEtool toolbox have been extensively compared with results from the literature in previous studies of cavities and fins [19–21]. For the sake of brevity, the verification is not repeated in this work.

3.1. Optimization Procedures

The constructal design method is employed to determine the restrictions, the degrees of freedom and the performance parameter of the evaluated flow system [1–4, 9, 31]. To obtain an optimal geometry for the seven degrees of freedom, the optimization process was performed with two distinct optimization methods: exhaustive search and Genetic Algorithm. The first part of the optimization process was performed using exhaustive search, which allows for a better analysis of the influence of the degree of freedom of interest over the system and allows for the calibration of the Genetic Algorithm for the subsequent optimizations. It was used for the first three degrees of freedom of the system (D_1/D_0, D_2/D_0, and D_3/D_0). A description of the main steps used for geometrical optimization in the present problem is depicted in Fig. 2, since definition of flow system with the constructal design up to optimization process. The description of the exhaustive search algorithm used in this work is presented in Fig. 3. For the second part of the optimization, i.e., for other degrees of freedom, only the Genetic Algorithm was utilized [34]. The description of the Genetic Algorithm used in the present work is shown in Fig. 4.

3.2. Genetic Algorithm Configurations

A genetic algorithm was used for the optimization of the fourth- and other higher-level degrees of freedom ($\tilde{D}_0$, H_2/D_0, L_1/D_0, and H/L). This change in optimization methods is mainly due to the unviability of the exhaustive search for higher-level optimizations due to the exponential increase of the numbers of simulations for each degree of freedom that is added. In this way, the Genetic Algorithm was calibrated with the results obtained from the exhaustive search optimization and then it was set to optimize the next degrees of freedom.

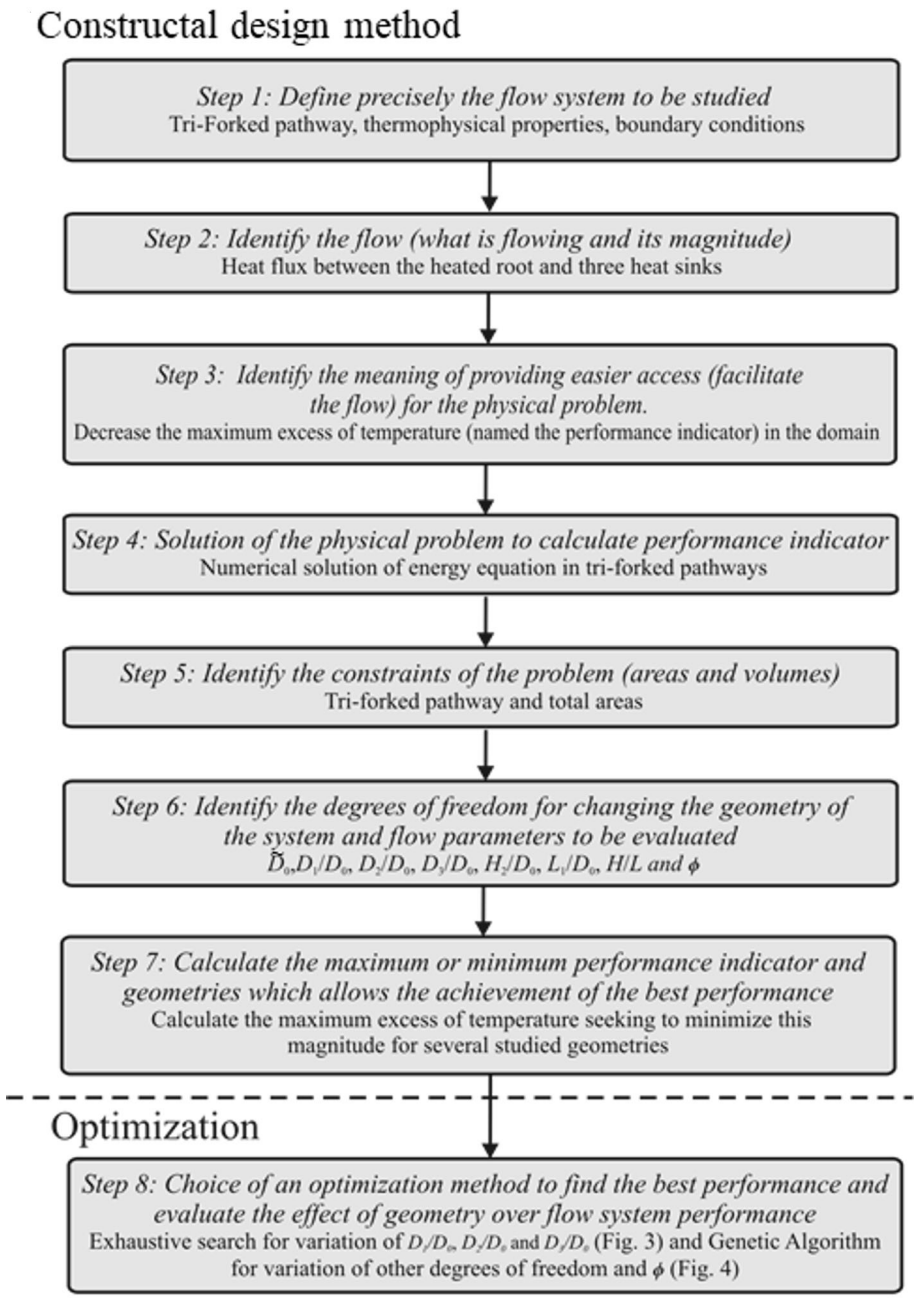

Fig. 2. Flowchart with application of constructal design and optimization methods for the present problem.

The validation and application of genetic algorithm on engineering problems have been extensively studied [34]. For the sake of brevity, this discussion is not shown here. The main parameters used for the binary, single-objective, elitist, Genetic Algorithm are shown in Table 2.

4. OPTIMAL TRI-FORKED PATHWAY GEOMETRY

The numerical work consisted of determining the temperature field in a large number of configurations of the type shown in Fig. 1. This same process of determining the temperature field was repeated in the present study for several values of $\tilde{D}_0$, D_1/D_0, D_2/D_0, D_3/D_0, H_2/D_0, L_1/D_0, H/L, and φ.

Algorithm 1. Exhaustive search-based optimization

$(\theta_{max})_m \leftarrow \infty$
$D_2/D_0 \leftarrow 0.5, D_3/D_0 \leftarrow 0.5, \widetilde{D}_0 \leftarrow 0.2, H_2/D_0 \leftarrow 2, L_1/D_0 \leftarrow 2, H/L \leftarrow 1, \phi \leftarrow 0.4$
for $d_1 \in \{0.01, 0.02, \ldots, 50\}$ **do**
    $y =\leftarrow maxTemperature(d_1, D_2/D_0, D_3/D_0, \widetilde{D}_0, H_2/D_0, L_1/D_0, H/L, \phi)$
    if $y < (\theta_{max})_m$
        $(\theta_{max})_m \leftarrow y$
        $(D_1/D_0)_o \leftarrow d_1$
$(\theta_{max})_{2m} \leftarrow \infty$
for $d_2 \in \{0.1, 0.2, \ldots, 10\}$ **do**
    for $d_1 \in \{0.01, 0.02, \ldots, 50\}$ **do**
        $y \leftarrow maxTemperature(d_1, d_2, D_3/D_0, \widetilde{D}_0, H_2/D_0, L_1/D_0, H/L, \phi)$
        if $y < (\theta_{max})_{2m}$
            $(\theta_{max})_{2m} \leftarrow y$
            $(D_1/D_0)_{2o} \leftarrow d_1$
            $(D_2/D_0)_o \leftarrow d_2$
$(\theta_{max})_{3m} \leftarrow \infty$
for $d_3 \in \{0.1, 0.2, \ldots, 10\}$ **do**
    for $d_2 \in \{0.1, 0.2, \ldots, 10\}$ **do**
        for $d_1 \in \{0.01, 0.02, \ldots, 50\}$ **do**
            $y \leftarrow maxTemperature(d_1, d_2, d_3, \widetilde{D}_0, H_2/D_0, L_1/D_0, H/L, \phi)$
            if $y < (\theta_{max})_{3m}$
                $(\theta_{max})_{3m} \leftarrow y$
                $(D_1/D_0)_{3o} \leftarrow d_1$
                $(D_2/D_0)_{2o} \leftarrow d_2$
                $(D_3/D_0)_o \leftarrow d_3$

Fig. 3. Exhaustive search algorithm used for the optimization of D_1/D_0, D_2/D_0, and D_3/D_0.

Table 2. Genetic algorithm parameters

Parameter	Value
Population size	40
Creation function	Uniform
Crossover function	Scattered
Mutation probability	5%
Crossover fraction	80%
Generations	200
Stall limit	20 generations

Figure 5 exhibits the effect of the ratio D_1/D_0 over the dimensionless maximum excess of temperature, θ_{max}, for various values of D_2/D_0, and for fixed values of $\tilde{D}_0 = 0.2$, $H/L = 1$, $\varphi = 0.4$, $H_2/D_0 = 2$, $L_1/D_0 = 2$, and $D_3/D_0 = 0.5$. Results show that the increase of the parameter D_2/D_0 improves significantly the thermal performance. The once minimized maximum excess of temperature for $D_2/D_0 = 0.5$ was $(\theta_{max})_m = 2.90225$, with $(D_1/D_0)_o = 0.56$. The best configuration was $(D_2/D_0)_o = 1.7$, where $(\theta_{max})_{2m} = 2.6793$, with $(D_1/D_0)_{2o} = 0.02$. Moreover, changes in the ratio D_2/D_0 also led to different effects of the ratio D_1/D_0 over the thermal performance of the tri-forked pathway. Note that the number of times minimized (or optimized) stands for the number of degrees of freedom that were considered in the analysis.

The optimal results shown in Fig. 5 are summarized in Fig. 6, which shows the effect of the middle

Algorithm 2. Genetic algorithm-based optimization

$H_2/D_0 \leftarrow 2, L_1/D_0 \leftarrow 2, H/L \leftarrow 1, \phi \leftarrow 0.4$
$D_1/D_0 \in \{0.01,0.02,\ldots,50\}, D_2/D_0 \in \{0.01,0.2,\ldots,10\}, D_3/D_0 \in \{0.01,0.2,\ldots,10\}$
for $d_0 \in \{0.10,0.15,\ldots,0.25\}$ ***do***
    $(\theta_{max})_{3m} \leftarrow GAscript(D_1/D_0, D_2/D_0, D_3/D_0, d_0, H_2/D_0, L_1/D_0, H/L, \phi)$
$\widetilde{D}_0 \in \{0.01,0.02,\ldots,0.99\}$
for $h_2 \in \{1.0, 1.5, \ldots, 3\}$ ***do***
    $(\theta_{max})_{4m} \leftarrow GAscript(D_1/D_0, D_2/D_0, D_3/D_0, \widetilde{D}_0, h_2, L_1/D_0, H/L, \phi)$
$H_2/D_0 \in \{0.1,0.2,\ldots,10\}$
for $l_1 \in \{0.5, 1.0, \ldots, 2\}$ ***do***
    $(\theta_{max})_{5m} \leftarrow GAscript(D_1/D_0, D_2/D_0, D_3/D_0, \widetilde{D}_0, H_2/D_0, l_1, H/L, \phi)$
$L_1/D_0 \in \{0.1,0.2,\ldots,10\}$
for $h \in \{0.1, 0.2, \ldots, 10\}$ ***do***
    $(\theta_{max})_{6m} \leftarrow GAscript(D_1/D_0, D_2/D_0, D_3/D_0, \widetilde{D}_0, H_2/D_0, L_1/D_0, h, \phi)$
$H/L \in \{0.1,0.2,\ldots,10\}$
for $phi \in \{0.3,0.4,0.5,0.6,0.7\}$ ***do***
    $(\theta_{max})_{7m} \leftarrow GAscript(D_1/D_0, D_2/D_0, D_3/D_0, \widetilde{D}_0, H_2/D_0, L_1/D_0, H/L, phi)$

Fig. 4. Genetic algorithm description used for the optimization of the remaining degrees of freedom.

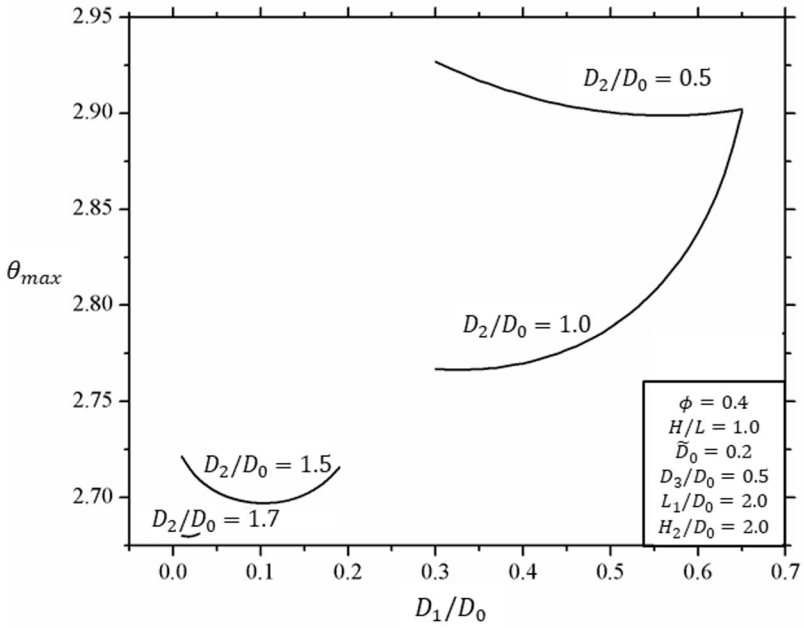

Fig. 5. Influence of the degree of freedom D_1/D_0 over the maximum excess temperature (θ_{max}) for different values of D_2/D_0.

sink size (D_2/D_0) over the once minimized maximum dimensionless temperature, $(\theta_{max})_m$, and its respective optimal ratio $(D_1/D_0)_o$. It can be seen a decrease of $(\theta_{max})_m$ with the increase of D_2/D_0. It is also noticed that the best configuration is the one with the smallest D_1/D_0, which can be interpreted as the system minimizing the left branch of the tri-forked pathway to achieve the best flow configuration. Figures 7a–7c illustrate the temperature distribution for the best configurations with: (a) $D_2/D_0 = 0.5$, (b) $D_2/D_0 = 1.0$, and (c) $(D_2/D_0)_o = 1.7$.

Next, the ratio D_3/D_0 was analyzed. Figure 8 shows the optimization of the twice optimized temperature $(\theta_{max})_{2m}$ as a function of the ratio D_3/D_0. It is noticed a great influence of the ratio D_3/D_0 over the twice minimized maximum dimensionless temperature, $(\theta_{max})_{2m}$, reducing it as the ratio

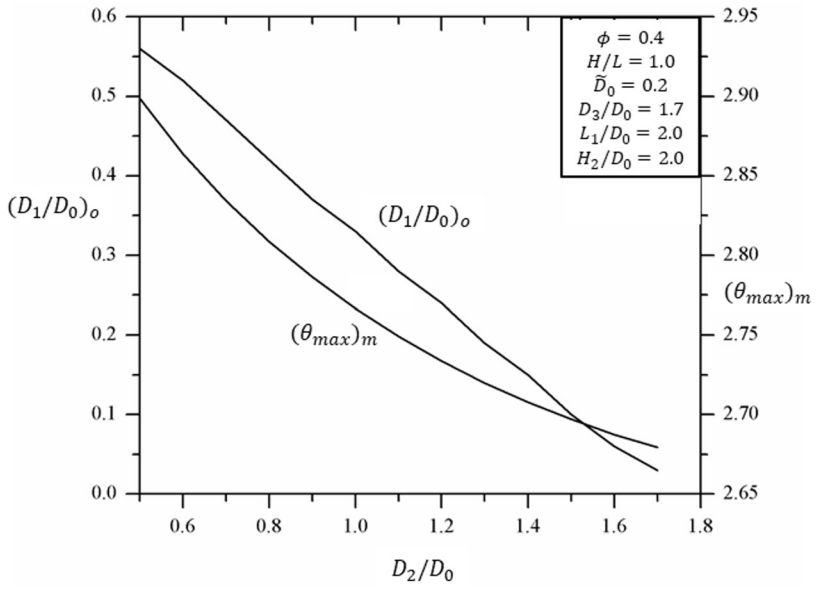

Fig. 6. Effect of the middle sink size (D_2/D_0) over the optimal left sink size $(D_1/D_0)_o$ and the optimal excess temperature $(\theta_{max})_m$.

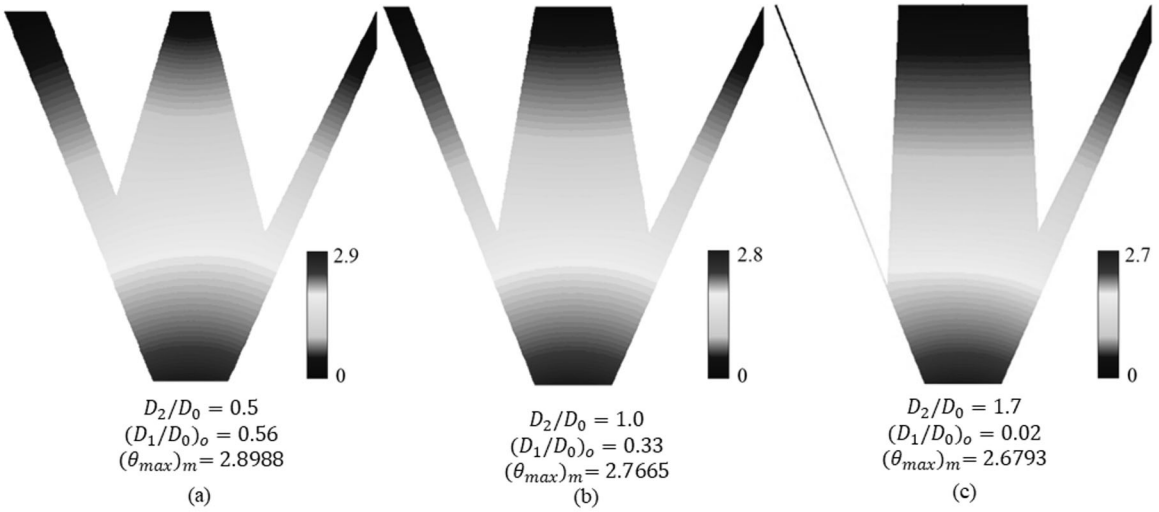

Fig. 7. Once-optimized geometries for: (a) $D_2/D_0 = 0.5$ and $(D_1/D_0)_o = 0.56$; (b) $D_2/D_0 = 1.0$ and $(D_1/D_0)_o = 0.33$; (c) $(D_2/D_0)_o = 1.7$, and $(D_1/D_0)_o = 0.02$. $(\theta_{max})_{2m} = 2.6793$ in (c) with $D_3/D_0 = 0.5$, $\tilde{D}_0 = 0.2$, $H_2/D_0 = L_1/D_0 = 2$, $H/L = 1$, and $\varphi = 0.4$.

increases. The value for the three times optimized maximum dimensionless temperature was $(\theta_{max})_{3m} = 2.1309$, obtained with the configuration of $(D_1/D_0)_{3o} = 0.01$, $(D_2/D_0)_{2o} = 0.1$, and $(D_3/D_0)_o = 3.2$. It is important to notice that the optimal ratio for the leftmost branch (D_1/D_0) remains basically constant and as small as the resolution previously defined. In addition, it is noticed a great reduction in the ratio of the middle branch of the pathway (D_2/D_0). It is worth mentioning that the optimal configuration is the one with the highest ratio D_3/D_0 and lowest ratios D_1/D_0 and D_2/D_0. This is because the system minimizes the heat transfer through these two pathways and dissipates most of the heat through the right branch. Figures 9a–9c show the optimal configurations for $D_3/D_0 = 1.0$, $D_3/D_0 = 2.0$, and $(D_3/D_0)_o = 3.2$, respectively. Up to this point, results showed that the definition of an asymmetric domain led to the generation of an optimal shape with high level of asymmetry. Then, it is clearly shown that the restriction of flow system domain has a higher influence over its generated shape.

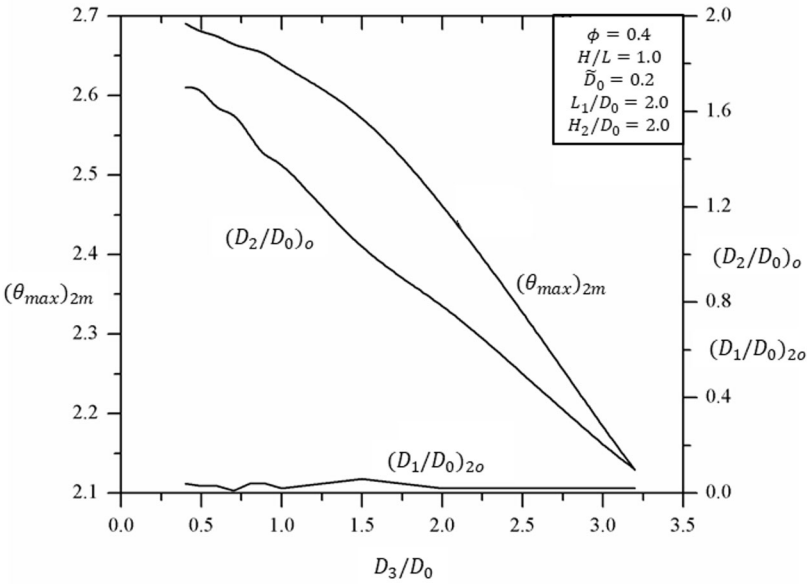

Fig. 8. Results from the third level of optimization, including the right sink size (D_3/D_0), showing the influence of this degree of freedom over the twice-minimized excess temperature $(\theta_{max})_{2m}$, on $(D_1/D_0)_{2o}$, as well as on the once-optimized middle sink $(D_2/D_0)_o$.

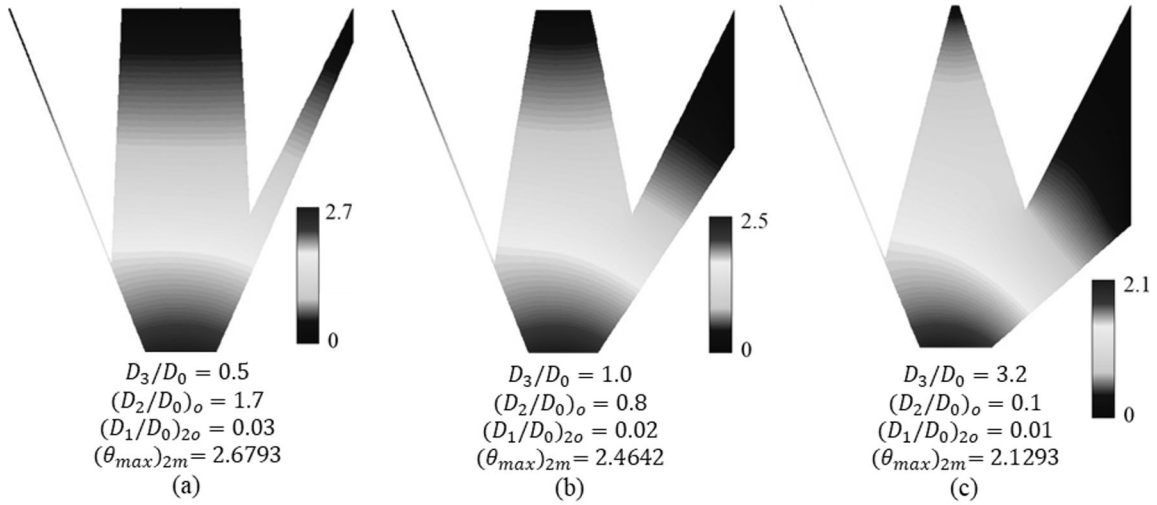

Fig. 9. Optimal topologies from the third optimization for: (a) $D_3/D_0 = 1.0$; (b) $D_3/D_0 = 2.0$; and (c) $D_3/D_0 = 3.2$, with $\tilde{D}_0 = 0.2$, $H_2/D_0 = L_1/D_0 = 2$, $H/L = 1$, and $\varphi = 0.4$.

For the subsequent degrees of freedom, $\tilde{D}_0$, H_2/D_0, L_1/D_0, H/L, the best configurations were found using genetic algorithm (GA) with the configurations previously described in Section 3.2.

The first degree of freedom optimized with GA was $\tilde{D}_0$, with $H_2/D_0 = L_1/D_0 = 2$, $H/L = 1$, and $\varphi = 0.4$. The results of the optimization are shown in Fig. 10a. From here onward, for clarity purposes, the influence on the previous degrees of freedom is not shown, as we are interested in the overall effect of each degree of freedom. The best configuration, illustrated in Fig. 10b, was found for $(\tilde{D}_0)_o = 0.13$, $(D_3/D_0)_{2o} = 7.8$, $(D_2/D_0)_{3o} = 0.1$, and $(D_1/D_0)_{4o} = 0.09$, resulting in a $(\theta_{max})_{4m} = 1.7729$. The found configuration shows that for these given degrees of freedom, the system adapts in such a way that it maintains a similar pattern, as found at the last step of optimization, i.e., still dissipating most of the heat received at the base through the right branch. However, opposite to the previous configuration, the middle branch is narrower, becoming less important in the process of heat diffusion.

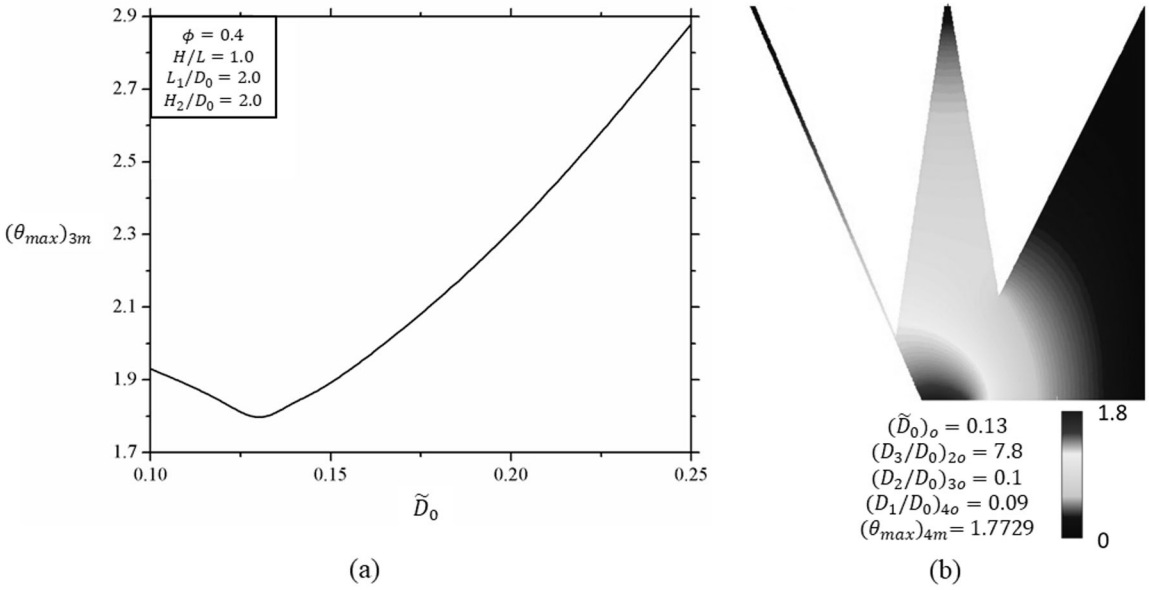

Fig. 10. (a) Optimization of $\tilde{D}_0$, showing the effect of the degree of freedom over the three times-optimized excess temperature; (b) topology of the optimal geometry for the fourth optimization level with $H_2/D_0 = L_1/D_0 = 2$, $H/L = 1$, and $\varphi = 0.4$.

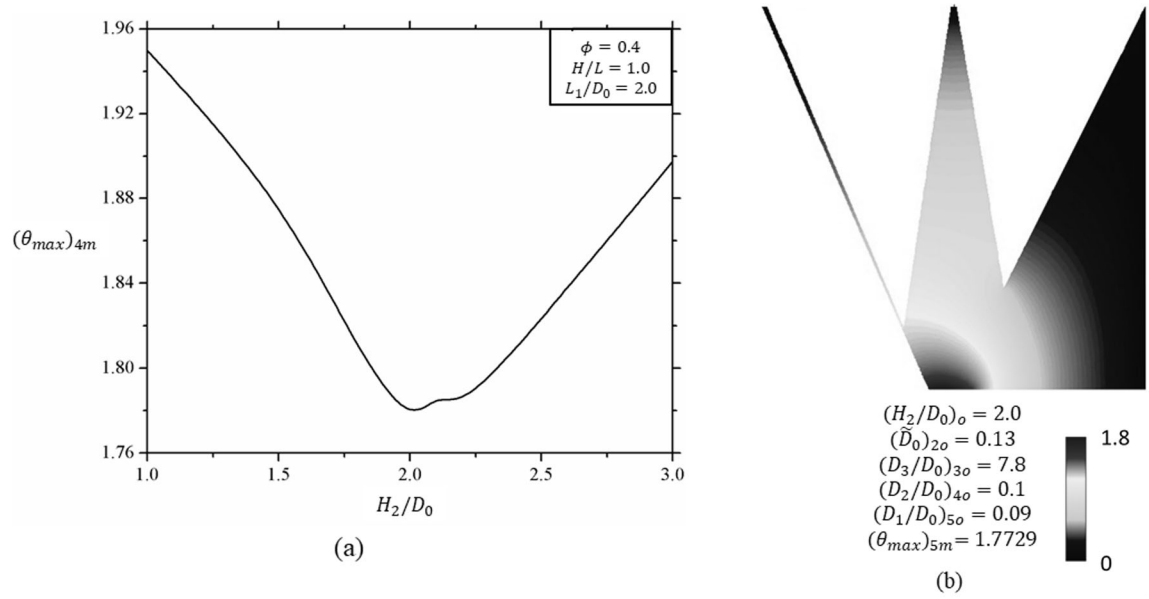

Fig. 11. (a) Optimization of H_2/D_0 showing the effect of the degree of freedom over the four times-optimized excess temperature; (b) topology of the optimal geometry for the fifth optimization level with $L_1/D_0 = 2$, $H/L = 1$, and $\varphi = 0.4$.

For the next degree of freedom, H_2/D_0 over the four times minimized maximum excess of temperature, $(\theta_{max})_{4m}$, is presented in Fig. 11a and the optimal configuration, shown in Fig. 11b, was found for $(H_2/D_0)_o = 2$, $(\tilde{D}_0)_{2o} = 0.13$, $(D_3/D_0)_{3o} = 7.8$, $(D_2/D_0)_{4o} = 0.1$ and $(D_1/D_0)_{5o} = 0.09$, resulting in a $(\theta_{max})_{5m} = 1.7729$ (for $L_1/D_0 = 2$, $H/L = 1$, and $\varphi = 0.4$). Coincidentally, this was the same geometry obtained at the last step of optimization, seen Fig. 10b. The influence of H_2/D_o over the $(\theta_{max})_{4m}$ shows that this parameter has influence over the dimensionless temperature. For the

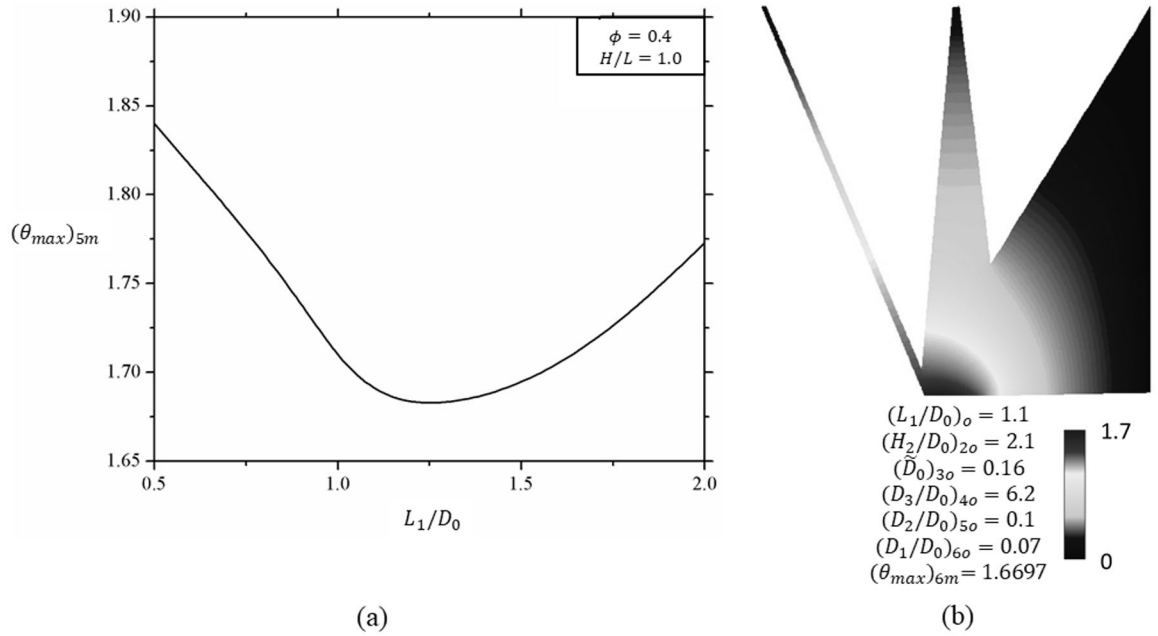

Fig. 12. (a) Optimization of L_1/D_0 showing the effect of the degree of freedom over the five times-optimized excess temperature; (b) topology of the optimal geometry for the sixth optimization level with $H/L = 1$ and $\varphi = 0.4$.

optimization of this degree of freedom, the system maintains the same behavior as seen in the previous optimization, still increasing the size of the right branch till the inferior limit when $\tilde{y} = 0$.

Afterwards, the optimization was performed for L_1/D_0 considering $H/L = 1.0$ and $\varphi = 0.4$, as shown in Fig. 12a. The optimal configuration was found for $(L_1/D_0)_o = 1.1, (H_2/D_0)_{2o} = 2.1, (\tilde{D}_0)_{3o} = 0.16$, $(D_3/D_0)_{4o} = 6.2$, $(D_2/D_0)_{5o} = 0.1$, and $(D_1/D_0)_{6o} = 0.07$, resulting in a $(\theta_{max})_{6m} = 1.6697$. The optimal configuration is shown in Fig. 12b. For this configuration, it is seen that the right branch is as large as possible, with the other branches a lot smaller in comparison. This happens because the right heat sink is the closest to the heat source, thus the system morphs in such a way to form a configuration where most of the heat is dissipated through that branch.

After that, the aspect ratio H/L was also considered as a degree of freedom to the system (Fig. 13a). The best configuration, shown in Fig. 13b, was found for $(H/L)_o = 0.1$, $(L_1/D_0)_{2o} = 1.6$, $(H_2/D_0)_{3o} = 0.1$, $(\tilde{D}_0)_{4o} = 0.7$, $(D_3/D_0)_{5o} = 0.1$, $(D_2/D_0)_{6o} = 1.4$, and $(D_1/D_0)_{7o} = 0.07$, resulting in a $(\theta_{max})_{7m} = 0.3994$. After allowing the system to change its slenderness factor, it is noticed that the system tries to become as short as possible, given that this configuration makes the middle heat sink closer to the heat source. With this, the system can dissipate the heat in a more efficient way through it. In addition, the contribution of lateral branches for heat exchange become peripheral, thus making them as thin as possible, and the configuration displaces toward a more symmetric shape.

Analyzing the results of the performance improvement over each optimization step, it is noticed that, for a fixed slenderness ratio (H/L), the rightmost branch ratio (D_3/D_0) was significantly greater than the other parameters, being three times more relevant than the optimization of D_2/D_0 and almost fifteen times more than $\tilde{D}_0$. This shows that the system optimizes itself relying a lot more on the adaptation of the branches and conditions imposed to them than the area in contact with the heat source itself, when it cannot change its height to length ratio. However, when allowing the freedom to change its slenderness, it is seen that this becomes dominant in the optimization of the case where you have a direct sink in the middle of the pathway, since it changes the shortest distance between the heat source and a heat sink.

After analyzing each optimization step and finding the best configuration for $\varphi = 0.4$, the same optimization was performed for different values of the area fraction. These results are shown in Fig. 14. As expected, the seven times minimized maximum excess of temperature decreases as the area ratio φ increases. This happens because there is more area available to exchange heat in the system. Figures 15a–15c illustrate the best geometries for $\varphi = 0.3$, 0.5, and 0.7, respectively. For $\varphi = 0.4$, it

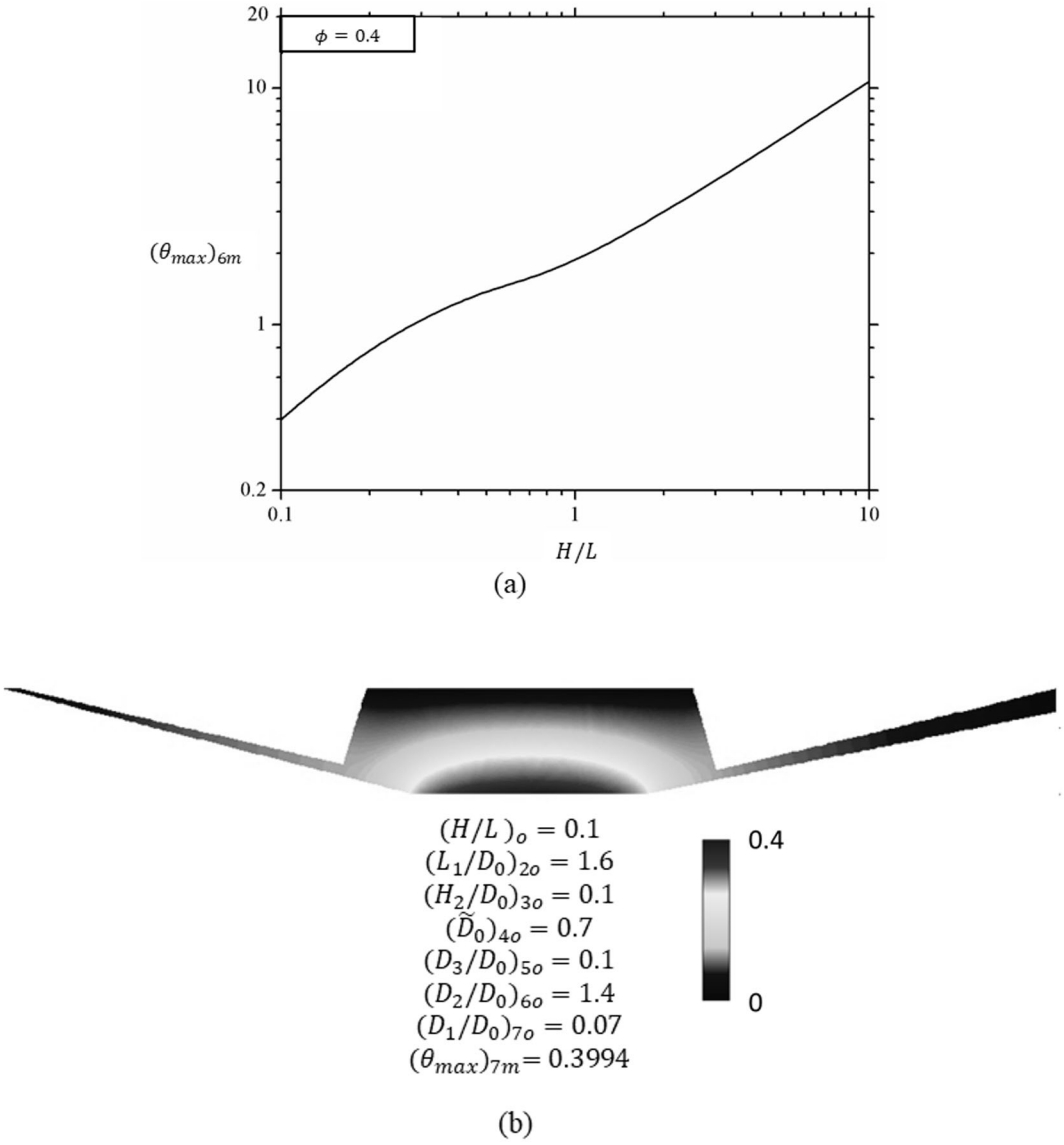

Fig. 13. Optimization of H/L showing: (a) the effect of the degree of freedom over the six times-optimized excess temperature; (b) topology of the optimal geometry for the seventh (and final) optimization level with $\varphi = 0.4$.

is already shown in Fig. 12. It can also be noticed that the increase of φ led to an augmentation of thickness of the central branch and reduces the participation of lateral branches in the heat transfer flux.

It is important to note that at each level of optimization, the system enhances its thermal performance. The fully optimized architecture has a maximum excess of temperature 6.27 times smaller than the once-optimized geometry, which is very significative. This result highlights the importance of the given degrees of freedom for the system in such a way to maximize the current access, as described by the constructal law. Also, results obtained here are compared with those found for a V-shaped considering the same thermal conditions and area fraction [31]. The maximum excess of temperature obtained for the tri-forked shape was 307% smaller than the one reached for the best V-shaped pathway. Results showed that, for the present thermal conditions, the increase of complexity led to a better thermal performance.

5. CONCLUDING REMARKS

Constructal design associated with a Genetic Algorithm was employed for geometrical optimization of a complex tri-forked pathway with seven degrees of freedom: D_1/D_0, D_2/D_0, D_3/D_0, $\tilde{D}_0$, H_2/D_0,

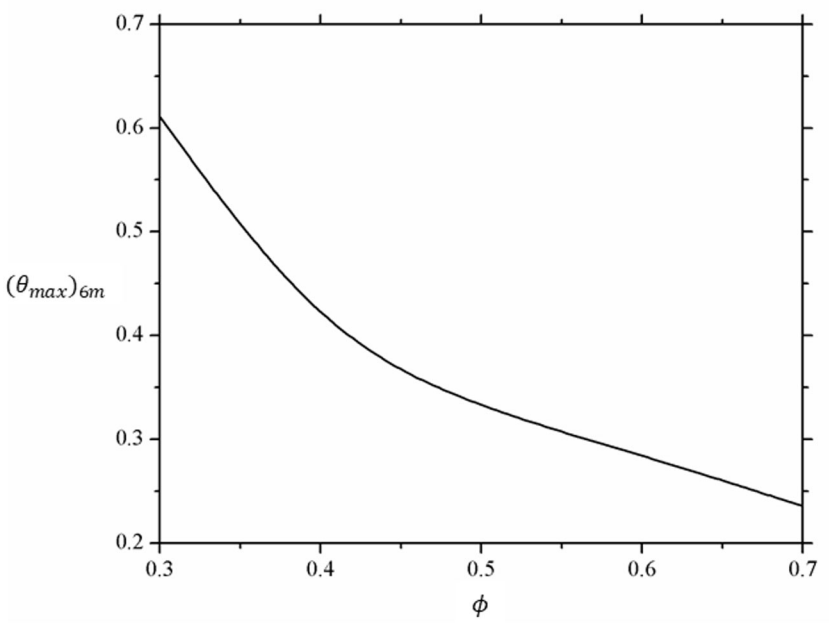

Fig. 14. Influence of the area ratio φ on the seven-times-minimized excess temperature $(\theta_{max})_{7m}$.

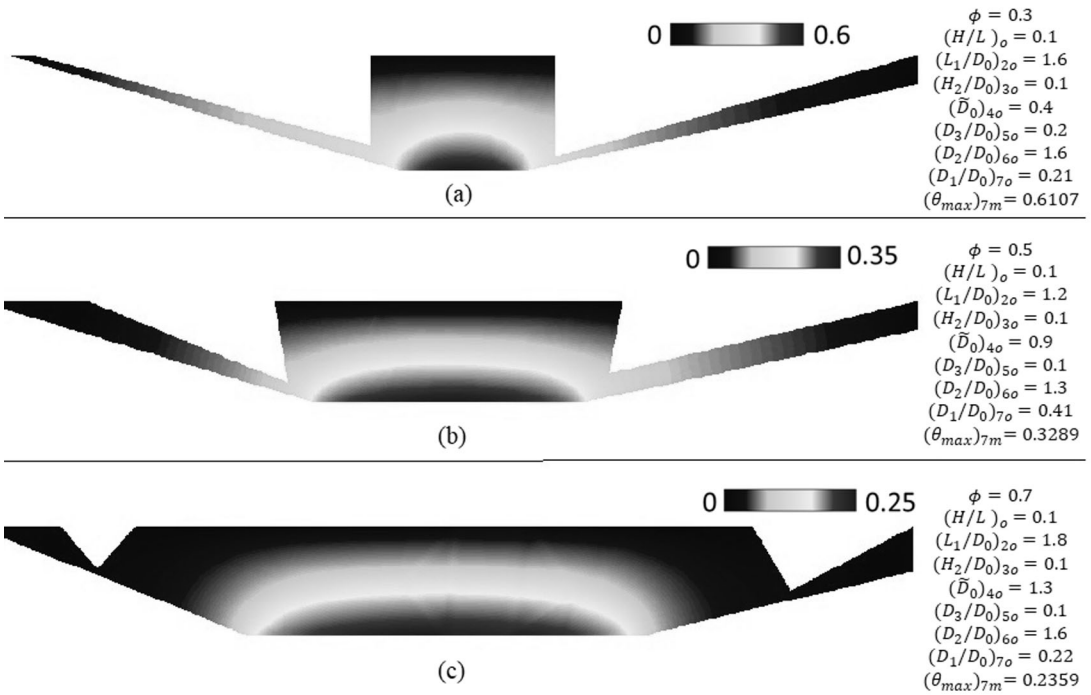

Fig. 15. Optimal geometries for: (a) $\varphi = 0.3$; (b) $\varphi = 0.5$; and (c) $\varphi = 0.7$.

L_1/D_0, and H/L. The focus point of the optimization was to minimize the global thermal resistance, represented by the maximum excess of temperature of the system. The tri-forked pathway was subject to two geometric constrains: the total area where the tri-forked pathway was inscribed (A) and the tri-forked pathway area (A_p). For the first part of the optimization, constructal design associated with exhaustive search provided the best configurations for the first three degrees of freedom. The effect of each degree of freedom over the system was analyzed. On the second part of the optimization, Genetic

Algorithm was used to extent the search of the optimal shapes for the other degrees of freedom. In addition, it allowed the analysis of the influence of the area ratio (φ) over the optimal geometry.

For the best geometry (with all degrees of freedom optimized), it was obtained an excess temperature of $(\theta_{max})_{7o} = 0.3994$ (for $\varphi = 0.4$), which accounts for an improvement of 627% over a one degree of freedom-optimized geometry, highlighting the importance of freedom for a flow system. The optimal tri-forked geometry has a 307% better performance over the optimal V-shaped geometry, showing that the tri-forked pathway is an evolution in design of the V-shaped pathway. Other important observation was obtained when the ratio H/L was varied. For higher ratios of H/L an asymmetrical optimal shape is achieved, while for lower ratios of H/L the bifurcated branches had low influence over thermal performance of the system.

Finally, other ideas arise from the present study. As the greatest improvement comes from reducing the distance between the base and the middle sink, a question that arises is concerned with the influence of different sink temperatures (or other thermal conditions) and its influence over thermal resistance of the system and its architecture. This will be analyzed in future works.

NOTATIONS

A—area [m^2]
D_0—length of single branch [m]
D_1—length of left branch [m]
D_2—length of central branch [m]
D_3—length of right branch [m]
H—height [m]
H_1—height of left branch [m]
H_2—height of right branch [m]
k—thermal conductivity [W m^{-1} K^{-1}]
L—length [m]
L_1—length of central branch at the branching point [m]
q—heat transfer rate [W]
T—temperature [K]
V—volume [m^3]
W—width [m]

Greek Symbols

θ—dimensionless temperature
φ—volume fraction

Subscripts

m—minimized
xm—x-times minimized
o—optimal
xo—x-times optimized
p—pathway
0—ambient

Superscript

($\tilde{}$) dimensionless variables

ACKNOWLEDGMENTS

The authors E.D. dos Santos, L.A. Isoldi, L.A.O. Rocha, and A.J. Silva Neto thank CNPq (Brasília, DF, Brazil) for research grant (processes: 306024/2017-9, 306012/2017-0, 307847/2015-2, 308363/2014-0). The authors also are grateful to FAPERGS, FAPERJ, and CAPES for financial support.

REFERENCES

1. Bejan, A. and Lorente, S., The Constructal Law and the Evolution of Design in Nature, *Phys. Life Rev.*, 2011, vol. 8, no. 3, pp. 209–240.
2. Bejan, A. and Zane, J.P., *Design in Nature*, New York: Doubleday, 2012.
3. Bejan, A. and Lorente, S., *Design with Constructal Theory*, Hoboken: Wiley, 2008.
4. Bejan, A., *Shape and Structure, from Engineering to Nature*, Cambridge: Cambridge University Press, 2000.
5. Bejan, A., Lorente, S., and Lee, J., Unifying Constructal Theory of Tree Roots, Canopies and Forests, *J. Theor. Biol.*, 2008, vol. 254, no. 3, pp. 529–540.
6. Reis, A.H. and Bejan, A., Constructal Theory of Global Circulation and Climate, *Int. J. Heat Mass Transfer*, 2006, vol. 49, nos. 11/12, pp. 1857–1875.
7. Miguel, A.F., The Emergence of Design in Pedestrian Dynamics: Locomotion, Self-Organization, Walking Paths and Constructal Law, *Phys. Life Rev.*, 2013, vol. 10, no. 2, pp. 168–190.
8. Bejan, A. and Merkx, G.W., *Constructal Theory of Social Dynamics*, New York: Springer, 2007.
9. Bejan, A., *The Physics of Life: The Evolution of Everything*, New York: St. Martins Press, 2016.
10. Bejan, A., Evolution in Thermodynamics, *Appl. Phys. Rev.*, 2017, vol. 4, no. 1, p. 011305.
11. Bejan, A., Maxwell's Demons Everywhere: Evolving Design as the Arrow of Time, *Sci. Rep.*, 2014, vol. 4, p. 4017.
12. Rodrigues, M.K., da S. Brum, R., Vaz, J., Rocha, L.A.O., dos Santos, E.D., and Isoldi, L.A., Numerical Investigation about the Improvement of the Thermal Potential of an Earth-Air Heat Exchanger (EAHE) Employing the Constructal Design Method, *Renew. Energy*, 2015, vol. 80, pp. 538–551.
13. Vieira, R.S., Petry, A.P., Rocha, L.A.O., Isoldi, L.A., and dos Santos, E.D., Numerical Evaluation of a Solar Chimney Geometry for Different Ground Temperatures by Means of Constructal Design, *Renew. Energy*, 2017, vol. 109, pp. 222–234.
14. Bello-Ochende, T., Olakoyejo, O.T., Meyer, J.P., Bejan, A., and Lorente, S., Constructal Flow Orientation in Conjugate Cooling Channels with Internal Heat Generation, *Int. J. Heat Mass Transfer*, 2013, vol. 57, pp. 241–249.
15. Teixeira, F.B., Lorenzini, G., Errera, M.R., Rocha, L.A.O., Isoldi, L.A., and dos Santos, E.D., Constructal Design of Triangular Arrangements of Square Bluff Bodies under Forced Convective Turbulent Flows, *Int. J. Heat Mass Transfer*, 2018, vol. 126, pp. 521–535.
16. Helbig, D., da Silva, C.C.C., Real, M. de V., dos Santos, E.D., Isoldi, L.A., and Rocha, L.A.O., Study about Buckling Phenomenon in Perforated Thin Steel Plates Employing Computational Modeling and Constructal Design Method, *Lat. Am. J. Solids Struct.*, 2016, vol. 13, pp. 1912–1936.
17. Martins, J.C., Goulart, M.M., Gomes, M. das, N., Souza, J.A., Rocha, L.A.O., Isoldi, L.A., and dos Santos, E.D., Geometric Evaluation of the Main Operational Principle of an Overtopping Wave Energy Converter by Means of Constructal Design, *Renew. Energy*, 2018, vol. 118, pp. 727–741.
18. Feijó, B.C., Lorenzini, G., Isoldi, L.A., Rocha, L.A.O., Goulart, J.N.V., and dos Santos, E.D., Constructal Design of Forced Convective Flows in Channels with Two Alternated Rectangular Heated Bodies, *Int. J. Heat Mass Transfer*, 2018, vol. 125, pp. 710–721.
19. Bejan, A. and Almogbel, M., Constructal T-Shaped Fins, *Int. J. Heat Mass Transfer*, 2000, vol. 43, no. 12, pp. 2101–2115.
20. Lorenzini, G. and Rocha, L.A.O., Constructal Design of Y-Shaped Assembly of Fins, *Int. J. Heat Mass Transfer*, 2006, vol. 49, no. 23, pp. 4552–4557.
21. Lorenzini, G. and Rocha, L.A.O., Constructal Design of T-Y Assembly of Fins for an Optimized Heat Removal, *Int. J. Heat Mass Transfer*, 2009, vol. 52, no. 5, pp. 1458–1463.
22. Xie, Z., Chen, L., and Sun, F., Constructal Optimization of Twice Y-Shaped Assemblies of Fins by Taking Maximum Thermal Resistance Minimization as Objective, *Sci. China Technol. Sci.*, 2010, vol. 53, no. 10, pp. 2756–2764.
23. Lorenzini, G., Biserni, C., and Rocha, L.A.O., Constructal Design of X-Shaped Conductive Pathways for Cooling a Heat-Generating Body, *Int. J. Heat Mass Transfer*, 2013, vol. 58, no. 1, pp. 513–520.
24. Hajmohammadi, M.R., Abianeh, V.A., Moezzinajafabadi, M., and Daneshi, M., Fork-Shaped Highly Conductive Pathways for Maximum Cooling in a Heat Generating Piece, *Appl. Therm. Eng.*, 2013, vol. 61, no. 2, pp. 228–235.

25. Horbach, C.S., dos Santos, E.D., Isoldi, L.A., and Rocha, L.A.O., Constructal Design of Y-Shaped Pathways for Cooling a Heat-Generating Body, *Defect Diffus. Forum*, 2014, vol. 348, no. 1, pp. 245–260.
26. Cheng, C.H. and Chen, Y.F., Topology Optimization of Heat Conduction Paths by a Non-Constrained Volume-of-Solid Function Method, *Int. J. Therm. Sci.*, 2014, vol. 78, pp. 16–25.
27. Lorenzini, G., Barreto, E.X., Beckel, C.C., Schneider, P.S., Isoldi, L.A., dos Santos, E.D., and Rocha, L.A.O., Constructal Design of I-Shaped High Conductive Pathway for Cooling a Heat-Generating Medium Considering the Thermal Contact Resistance, *Int. J. Heat Mass Transfer*, 2016, vol. 93, pp. 770–777.
28. Lorenzini, G., Barreto, E.X., Beckel, C.C., Schneider, P.S., Isoldi, L.A., dos Santos, E.D., and Rocha, L.A.O., Geometrical Evaluation of T-Shaped High Conductive Pathway with Thermal Contact Resistance for Cooling of Heat-Generating Medium, *Int. J. Heat Mass Transfer*, 2017, vol. 108, pp. 1884–1893.
29. You, J., Feng, H., Chen, L., and Xie, Z., Heat Conduction Constructal Optimization for Nonuniform Heat Generating Area Based on Triangular Element, *Int. J. Heat Mass Transfer*, 2018, vol. 117, pp. 896–902.
30. Cetkin, E. and Oliani, A., The Natural Emergence of Asymmetric Tree-Shaped Pathways for Cooling of a Non-Uniformly Heated Domain, *J. Appl. Phys.*, 2015, vol. 118, no. 2, p. 024902.
31. Estrada, E. da. S.D., Fagundes, T.M., Isoldi, L.A., dos Santos, E.D., Xie, G., and Rocha, L.A.O., Constructal Design Associated to Genetic Algorithm of Asymmetric V-Shaped Pathways, *J. Heat Transfer*, 2015, vol. 137, no. 6, p. 061010.
32. *MATLAB, 2000, User's Guide*, Vers. 6.0.088, Release 12, Natick, MA: The Mathworks, 2000.
33. Reddy, J.N. and Gartling, D.K., *The Finite Element Method in Heat Transfer and Fluid Dynamics*, Florida: CRC, 1994.
34. Gosselin, L., Tye-Gingras, M., and Mathieu-Potvin, F., Review of Utilization of Genetic Algorithms in Heat Transfer Problems, *Int. J. Heat Mass Transfer*, 2009, vol. 52, nos. 9/10, pp. 2169–2188.